

Liquidus phase relationships on the join anorthite-forsterite-quartz at 10 kbar with applications to basalt petrogenesis*

G. Sen** and D.C. Presnall

Department of Geosciences, University of Texas at Dallas, P.O. Box 688, Richardson, Texas 75080, USA

Abstract. Liquidus phase relationships determined on the join $\text{CaAl}_2\text{Si}_2\text{O}_8$ (anorthite)– Mg_2SiO_4 (forsterite)– SiO_2 (quartz) at 10 kbar show that increasing pressure causes the forsterite and anorthite primary phase fields to shrink and the spinel, enstatite and silica fields to expand. The boundary line between the enstatite and forsterite fields and that between the enstatite and quartz fields both move away from the SiO_2 apex as pressure increases. Therefore, simplified source peridotite would yield simplified basaltic partial melts with decreasing silica as pressure increases, as has been found in other studies. Also, increasing pressure decreases the amount of silica enrichment in residual liquids produced by fractional crystallization. Although anorthite is unstable in simplified peridotite above 9 kbar in the system $\text{CaO}–\text{MgO}–\text{Al}_2\text{O}_3–\text{SiO}_2$, it is an important phase in the fractional crystallization of simplified basalts at 10 kbar and probably also in natural basalts.

a simplified analog of the tholeiitic portion of the basalt tetrahedron of Yoder and Tilley (1962). Viewed from either compositional or mineralogical relationships, the CMAS system is particularly valuable in modeling the generation and crystallization of basalts because (1) it contains about 85% of the chemical constituents of basalt and about 90% of the chemical constituents of their peridotite source rocks in the mantle, and (2) it contains representatives of all the major anhydrous phases of basalts and peridotites.

As part of a systematic program in this laboratory aimed at clarifying liquidus phase relationships in the system forsterite-diopside-anorthite-quartz as a function of pressure, we present here liquidus relationships on the join anorthite-forsterite-quartz at 10 kbar. This join forms the base of the tholeiitic part of the simplified basalt tetrahedron in the CMAS system.

Introduction

In the early high temperature phase equilibrium studies at the Geophysical Laboratory, one of the first ternary systems to be determined was anorthite-forsterite-silica (Andersen 1915). This system was considered to be important to studies of the crystallization behavior of basalts because it shows the combined effect of the crystallization of anorthite and the reaction relation of forsterite with liquid to form enstatite. Thus, it represents a reasonably close ternary analog to the crystallization behavior of basalts.

More recently, the system $\text{CaO}–\text{MgO}–\text{Al}_2\text{O}_3–\text{SiO}_2$ (CMAS) has been used as a simplified model system approximating phase relationships in basalts and their peridotite source rocks (O'Hara 1965, 1968; O'Hara and Yoder 1967; Presnall et al. 1978, 1979). Within this 4-component system, studies have been concentrated on the tetrahedron Mg_2SiO_4 (forsterite)– $\text{CaMgSi}_2\text{O}_6$ (diopside)– $\text{CaAl}_2–\text{Si}_2\text{O}_8$ (anorthite)– SiO_2 (quartz), which has been used as

Experimental method

For each starting mixture, 10 g of material were prepared from pure, dried oxides as described by Presnall et al. (1972). Each mixture was fired twice in a Pt crucible for 4 h with one intermediate crushing and remixing, and then quenched to a glass.

Runs were carried out in a solid media piston-cylinder apparatus as described by Presnall et al. (1973), except that Pyrex glass sleeves were used in place of boron nitride sleeves. Temperatures are corrected to the International Practical Temperature Scale of 1968 (Anonymous 1969). Charges were contained in Pt capsules and all assembly parts, except for the talc and glass sleeves, were dried for 1 h at 1,050° C so as to keep the charges free of water. The glass sleeves were stored in an oven at 110° C.

All experiments were of the piston-out type (Presnall et al. 1978) and no pressure correction was applied. In all cases, W3Re/W25Re thermocouples were used. Phases were identified microscopically in reflected light, and their compositions were determined with an automated (Tracor-Northern NS-880) electron microprobe (ARL model EMX) at the University of California at Los Angeles. Operating conditions were 15 kilovolts accelerating potential, 100 microamps emission current, 30 nanoamps beam current and a one micron beam diameter. The wavelength-dispersive method was used in all cases, and the raw data were reduced to compositions using the Bence-Albee correction procedure.

* Contribution no. 419, Department of Geosciences, University of Texas at Dallas

** Present address: Department of Earth and Space Sciences, University of California at Los Angeles, Los Angeles, California 90024, USA

Previously in this laboratory, boron nitride sleeves were used in the pressure cell assembly. When glass sleeves are used, liquidus temperatures are slightly higher and microprobe analyses of glass phases do not show the slightly low summations (98–99.5%) that almost always occur with runs using boron nitride sleeves. We infer from these results that hydrogen originating from dehydration of the talc diffuses through the boron nitride and Pt capsule wall into the run. There it combines with oxygen to form water, which depresses the liquidus temperature. Glass sleeves appear to be a much more effective shield against hydrogen diffusion than boron nitride.

Chen and Presnall (1975) found that the melting of Pt capsules far below the normal melting point of Pt (Boyd and England 1963, p 314; Presnall et al. 1973, Fig. 6) is caused by alloying of the Pt capsule with Si and that the source of Si lies inside the capsule. Loss of Si from the charge to the capsule is probably made possible by the presence of hydrogen which takes up the free oxygen and forms water. Thus, it appears that if the charges are maintained free of hydrogen, Pt capsules can be used for runs of indefinite length, even at very high temperatures.

With glass sleeves we have redetermined liquidus temperatures in some of the older work reported from this laboratory in which boron nitride sleeves were used (Chen and Presnall 1975; Presnall 1976; Presnall et al. 1978, 1979) and we find that temperature errors are marginally detectable at 10 kbar and are about 20° C at 20 kbar. Thus, we conclude that temperatures for liquidus and solidus transitions in these older papers should be raised about 1° C/kbar. The positions of liquidus phase boundaries in the older data appear not in need of revision.

Reversal experiments

Other factors being equal, the rate of attainment of crystal-liquid equilibrium tends to be characteristic of the particular crystalline phase. Therefore, following the procedure of Presnall et al. (1978), we have reversed one liquidus bracket for each of the primary phase fields (except corundum, which was not attempted) and have assumed that other experiments extending for times as long or longer than the reversal experiments attained equilibrium. Reversals were obtained independently of either the character of the starting mixture or the method of approach to the run conditions by first bracketing a liquidus temperature with runs of, say, 8 h. A pair of experiments was then carried out in which the charge was held either below or above the liquidus temperature for 8 h and then, without taking the charge out of the apparatus, the temperature was changed to the other side of the liquidus and held for an additional 8 h. As shown in Table 1, 8 h runs were adequate to obtain equilibrium for all primary phase fields except that of β quartz. For the β quartz field, 24 h runs were necessary.

Phase relationships at 10 kbar

The liquidus surface of the join anorthite-forsterite-quartz at 10 kbar is shown in Fig. 1. It is based on quenching experiments and glass analyses given in Tables 2 and 3. Because of solid solution of Al in enstatite (Table 4) and the fact that spinel lies off the join, the only ternary boundary line is the one separating the anorthite and β quartz

Table 1. Reversal experiments

Run no.	Initial conditions		Final conditions		Run products ^a
	T (°C)	Duration (h)	T (°C)	Duration (h)	
52% CaAl ₂ Si ₂ O ₈ , 15% Mg ₂ SiO ₄ , 33% SiO ₂ ^b (GS-3)					
304-6	1,340	24	1,400	24	gl
304-13	1,400	24	1,340	24	gl + qz + en + an
55% CaAl ₂ Si ₂ O ₈ , 35% Mg ₂ SiO ₄ , 10% SiO ₂ (GS-0)					
303-11	1,390	8	1,450	8	gl
303-9	1,450	8	1,390	8	gl + fo + sp
60% CaAl ₂ Si ₂ O ₈ , 23% Mg ₂ SiO ₄ , 17% SiO ₂ (GS-2)					
304-7	1,330	8	1,390	8	gl
304-8	1,390	8	1,330	8	gl + en
67% CaAl ₂ Si ₂ O ₈ , 17% Mg ₂ SiO ₄ , 16% SiO ₂ (GS-5)					
303-2	1,390	8	1,450	8	gl
303-3	1,450	8	1,390	8	gl + an

^a gl = glass, fo = forsterite, en = enstatite, qz = β quartz, sp = spinel, an = anorthite

^b Mineral proportions in weight percent

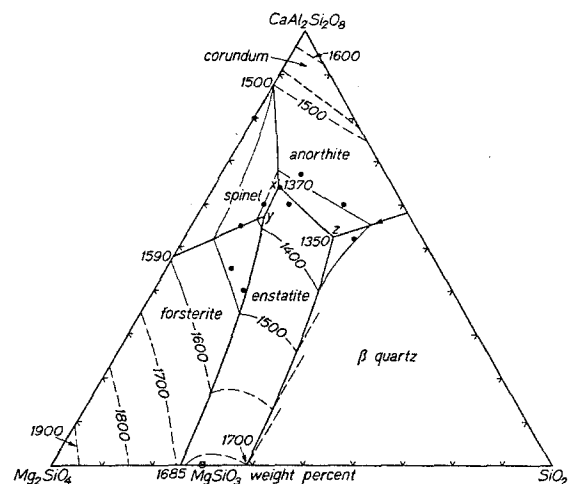


Fig. 1. Liquidus surface of the join CaAl₂Si₂O₈ (anorthite)–Mg₂SiO₄ (forsterite)–SiO₂ (quartz) at 10 kbar. Data on the bounding binary systems anorthite-quartz and forsterite-quartz, and on the bounding join forsterite-anorthite are from Clark et al. (1961), Chen and Presnall (1975) and Presnall et al. (1978), respectively. Liquidus temperatures from the latter two references have been raised 10° C (see text). The arrow showing the direction of decreasing temperature on the β quartz-anorthite boundary line indicates that this boundary line is ternary. Others are not

primary phase fields. The possibility of more than one Ca-pyroxene primary phase field has not been examined.

The diagram at 10 kbar shows three piercing points (x , y , z) at which the phases an + en + sp + liq, fo + en + sp + liq, and an + en + qz + liq, respectively, are in equilibrium. Two of these (x , y) were located by the classical procedure of bracketing them between liquidus primary phase determinations for nearby bulk compositions. The third (z) was determined by electron microprobe analysis. One run (Tables 2 and 3, run 304-9) yielded the assemblage enstatite + anor-

Table 2. Quenching experiments

Run no.	Temperature (°C)	Duration (h)	Run products ^a
40% CaAl ₂ Si ₂ O ₈ , 60% MgSiO ₃ ^b			
303-7	1,500	8	gl
303-10	1,480	8	gl + fo
60% CaAl ₂ Si ₂ O ₈ , 40% MgSiO ₃			
303-5	1,410	9	gl
303-4	1,390	8	gl + sp
303-13	1,360	48	gl + sp + en
303-14	1,355	49	sp + en + an
80% CaAl ₂ Si ₂ O ₈ , 20% Mg ₂ SiO ₄			
302-13	1,570	4	gl
302-14	1,550	4	gl + sp
45% CaAl ₂ Si ₂ O ₈ , 42% Mg ₂ SiO ₄ , 13% SiO ₂ (GS-1)			
302-11	1,510	9	gl
302-12	1,490	8	gl + fo
52% CaAl ₂ Si ₂ O ₈ , 15% Mg ₂ SiO ₄ , 33% SiO ₂ (GS-3)			
303-15	1,380	24	gl
303-12	1,400	24	gl + qz
55% CaAl ₂ Si ₂ O ₈ , 35% Mg ₂ SiO ₄ , 10% SiO ₂ (GS-0)			
301-11	1,430	8	gl
301-10	1,410	8	gl + fo + sp
301-2	1,370	48	gl + fo + sp
60% CaAl ₂ Si ₂ O ₈ , 23% Mg ₂ SiO ₄ , 17% SiO ₂ (GS-2)			
301-9	1,370	11	gl
301-12	1,350	8	gl + en
60% CaAl ₂ Si ₂ O ₈ , 12% Mg ₂ SiO ₄ , 28% SiO ₂ (GS-6)			
300-14	1,400	8	gl
301-3	1,380	9	gl + an
304-9	1,350	48	gl + an + en + qz
304-10	1,345	48	gl + an + en + qz
302-10	1,340	48	an + en + qz
64% CaAl ₂ Si ₂ O ₈ , 23% Mg ₂ SiO ₄ , 13% SiO ₂ (GS-11)			
301-14	1,370	10	gl
302-4	1,368	49	gl + an + en
302-2	1,365	48	gl + an + en + sp
302-1	1,360	49	gl + an + en + sp
67% CaAl ₂ Si ₂ O ₈ , 17% Mg ₂ SiO ₄ , 16% SiO ₂ (GS-5)			
301-15	1,430	8	gl
301-13	1,410	11	gl + an
300-8	1,260	48	an + en + qz

^a Abbreviations same as in Table 1^b Mixture proportions in weight percent

thite + β quartz + glass, and the analyzed glass had a composition exactly on the plane of the diagram. This composition was therefore used for point z. Another run (Tables 2 and 3, run 304-10) yielded the same phase assemblage at a temperature just 5 degrees lower. The composition of the glass in this run contains a small amount of normative diopside (Table 3) and helps locate the position of the isobaric quaternary univariant line en + an + qz + liq within the tetrahedron forsterite-diopside-anorthite-quartz. The position of this line in the tetrahedron is shown in two projections in Fig. 2. Compositions of the three piercing

Table 3. Glass compositions (weight percent)

Run no.	304-9	304-10
No. of spots analyzed	6	5
SiO ₂	59.8 (0.8) ^a	60.1 (0.3)
Al ₂ O ₃	19.1 (0.3)	18.6 (0.3)
MgO	10.2 (0.5)	9.1 (0.2)
CaO	10.5 (0.2)	11.5 (0.4)
Sum	99.3	99.6
di	—	4.9
an	52.3	51.1
fo	17.9	14.4
q	29.8	29.6

^a Values in parentheses are mean deviations**Table 4.** Enstatite compositions

Run no.	302-2	304-10
SiO ₂	55.50	54.62
Al ₂ O ₃	6.38	8.62
MgO	36.41	36.11
CaO	1.61	1.26
Sum	99.90	100.61
Number of cations for 6 oxygens		
Si	1.868	1.824
Al (IV)	0.132	0.176
Al (VI)	0.121	0.163
Mg	1.827	1.798
Ca	0.058	0.045
Sum	4.006	4.006

points are located at 64% an, 23% fo, 13% qz (x), 57.5% an, 29% fo, 13.5% qz (y) and 52.3% an, 17.9% fo, 29.8% qz (z).

Table 4 shows two aluminous enstatite compositions. The analysis in the first column is an enstatite in equilibrium with a liquid on the isobaric univariant line enstatite + spinel + anorthite + liquid. The glass in this run was not analyzed but its composition must lie very close to point x (Fig. 1) and slightly off the anorthite-forsterite-quartz plane toward diopside. The second column shows an enstatite in equilibrium with a liquid on the isobaric univariant line enstatite + anorthite + β quartz + liquid. The glass composition is given in Table 3 and shown in Fig. 2. In both runs, crystals suitable for analysis were difficult to find and the compositions given are based on analysis of only one crystal in each run. Therefore, we consider these analyses to be only approximate.

In Fig. 5, the liquidus phase boundaries at 10 kbar are compared with those at one atm determined by Andersen (1915) as modified by Irvine (1975). Longhi (1978) showed another revision of this diagram with the piercing points for anorthite + enstatite + β quartz + liquid and anorthite + forsterite + enstatite + liquid both shifted slightly toward the SiO₂ apex. As the runs of Andersen were at most only

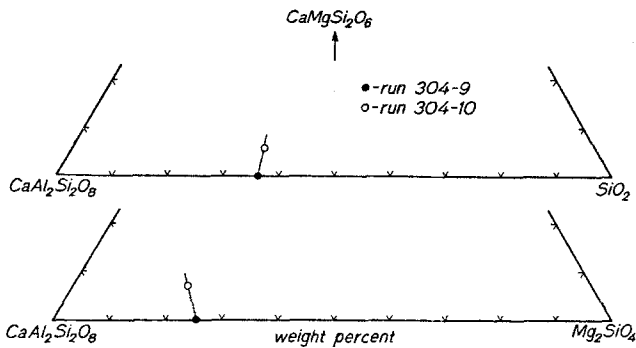


Fig. 2. Projections of analyzed glass compositions along the isobaric quaternary univariant line enstatite + anorthite + β -quartz + liquid. The $\text{CaMgSi}_2\text{O}_6$ – $\text{CaAl}_2\text{Si}_2\text{O}_8$ – SiO_2 diagram is projected from Mg_2SiO_4 , and the $\text{CaMgSi}_2\text{O}_6$ – $\text{CaAl}_2\text{Si}_2\text{O}_8$ – Mg_2SiO_4 diagram is projected from SiO_2 .

two hours long, it seems likely that the revision of Longhi is correct. Nevertheless, we have not used his revision because the data supporting it are not yet published.

As has been found in earlier studies on similar systems, increasing pressure causes the forsterite and anorthite fields to shrink and the spinel, enstatite and quartz fields to expand. It will be noticed that the two piercing points *a* and *b* at 1 atm are exchanged at 10 kbar for the piercing points *x* and *y*. This is caused by the fact that the isobaric quaternary invariant point involving the phases forsterite, enstatite, spinel, anorthite and liquid changes position as pressure increases. At pressures below 5 kbar, it lies on the diopside-deficient side of the join anorthite-forsterite-quartz. It lies on this join at an interpolated pressure of about 5 kbar and lies within the tholeiitic basalt tetrahedron at higher pressures (see point *n* in Fig. 8 of Presnall et al. 1979). At pressures above 9 kbar, it no longer exists (Presnall et al. 1979).

Petrological implications

In the join anorthite-forsterite-quartz, the closest approximation to a peridotite source rock would be a mixture consisting mainly of forsterite and enstatite and lying near the forsterite-quartz base of the triangle. As shown in Fig. 3, the boundary line between forsterite and enstatite shifts away from the quartz apex as pressure increases, so primary magmas derived from the simplified mantle would become progressively more depleted in SiO_2 . Thus, the data on this join are in agreement with other studies in this pressure range (for example O'Hara 1965, 1968; Green and Ringwood 1967; Kushiro 1968; Presnall et al. 1978, 1979; Chen and Presnall 1975; Stolper 1980).

Another application of the data concerns the reaction $\text{fo} + \text{liq} = \text{en} + \text{sp}$ at the piercing point *y*. Reaction rims of hypersthene and magnetite around olivine have been reported by several investigators (Kuno 1950, p 970; Muir et al. 1957, Fig. 4; Snyder 1959, p 192; Yoder and Tilley 1962, p 425). These compound reaction rims were attributed by Kuno (1950) to reaction of olivine with the enclosing liquid but Yoder and Tilley (1962) attributed them to oxidation of olivine without participation of liquid in the reaction. Presnall (1966) showed that the reaction $\text{ol} + \text{liq} = \text{en} + \text{sp}$ occurs in the system $\text{CaO} - \text{MgO} - \text{FeO} - \text{Fe}_2\text{O}_3 - \text{SiO}_2$ and concluded that at least some of the reaction rims

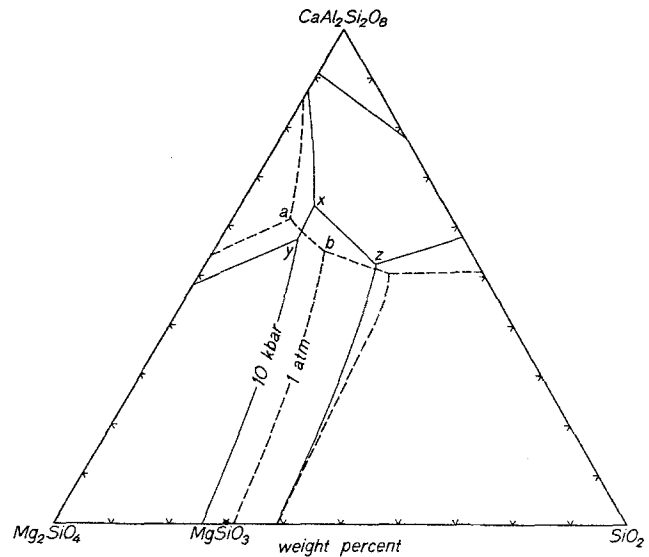


Fig. 3. Comparison of liquidus phase boundaries at 10 kbar with those at 1 atm (Andersen 1915, as modified by Irvine 1975)

found in lavas are due to reaction of olivine with liquid. The fact that this reaction also occurs on the join forsterite-anorthite-silica further reinforces this conclusion.

A final application of the data concerns the fractional crystallization of basaltic magmas. In the system forsterite-silica, Chen and Presnall (1975) showed that the eutectic between enstatite and silica remains essentially constant in composition over the pressure range of 1 atm to 25 kbar. However, when anorthite is added to this system, the piercing point involving the phases enstatite, quartz, anorthite and liquid (Fig. 3) moves away from the silica apex as pressure increases. Thus, high pressures not only cause the production of less siliceous primary basaltic magmas, but it appears likely that the fractional crystallization of these basalts at high pressures yields less siliceous final crystallization products. An interesting feature of the phase relationships at 10 kbar is the fact that anorthite is no longer stable in the source peridotite from which simplified basalts would be derived. Nevertheless, anorthite is an important phase involved in the fractional crystallization of simplified basalts and probably also natural basalts at this pressure. This conclusion is consistent with the results of O'Hara et al. (1970) on a lunar basalt.

Acknowledgements. This research was supported by National Science Foundation Grants EAR-78-22766, EAR 8018359, and EAR-8212889 to D.C. Presnall. Part of the costs of manuscript preparation were supported by the U.S. Geological Survey, Reston, Virginia, during the tenure of a leave of absence by Presnall from the University of Texas at Dallas.

References

- Andersen O (1915) The system anorthite-forsterite-silica. *Am J Sci* 4th Ser 39:407–454
- Anonymous (1969) The international practical temperature scale of 1968. *Metrologia* 5:35–44
- Boyd FR, England JL (1963) Effect of pressure on the melting of diopside, $\text{CaMgSi}_2\text{O}_6$, and albite, $\text{NaAlSi}_3\text{O}_8$, in the range up to 50 kilobars. *J Geophys Res* 68:311–323
- Chen C-H, Presnall DC (1975) The system $\text{Mg}_2\text{SiO}_4 - \text{SiO}_2$ at pressures up to 25 kilobars. *Am Mineral* 60:398–406

- Clark SP, Schairer JF, de Neufville J (1962) Phase relations in the system $\text{CaMgSi}_2\text{O}_6$ – $\text{CaAl}_2\text{Si}_2\text{O}_6$ – SiO_2 at low and high pressures. *Yearb Carnegie Inst Washington* 61:59–68
- Green DH, Ringwood AE (1967) The genesis of basaltic magmas. *Contrib Mineral Petrol* 15:103–190
- Irvine TN (1975) Olivine-pyroxene-plagioclase relations in the system Mg_2SiO_4 – $\text{CaAl}_2\text{Si}_2\text{O}_8$ – KAlSi_3O_8 – SiO_2 and their bearing on the differentiation of stratiform intrusions. *Yearb Carnegie Inst Washington* 74:492–500
- Kuno H (1950) Petrology of Hakone volcano and the adjacent areas, Japan. *Geol Soc Am Bull* 61:957–1020
- Kushiro I (1968) Compositions of magmas formed by partial zone melting of the earth's upper mantle. *J Geophys Res* 73:619–634
- Longhi J (1978) Pyroxene stability and the composition of the lunar magma ocean. *Proc Lunar Sci Conf*, 9th, 285–306
- Muir ID, Tilley CE, Scoon JH (1957) Contributions to the petrology of Hawaiian basalts. I. The picrite basalts of Kilauea. *Am J Sci* 255:241–253
- O'Hara MJ (1965) Primary magmas and the origin of basalts. *Scot J Geol* 1:19–40
- O'Hara MJ (1968) The bearing of phase equilibria studies in synthetic and natural systems on the origin and evolution of basic and ultrabasic rocks. *Earth Sci Revs* 4:69–133
- O'Hara MJ, Yoder HS, Jr (1967) Formation and fractionation of basic magmas at high pressures. *Scot J Geol* 3:67–117
- O'Hara MJ, Biggar GM, Richardson SW, Ford CE, Jamieson BG (1970) The nature of seas, mascons and the lunar interior in the light of experimental studies. *Proc Appolo 11 Lunar Sci Conf*, 695–710
- Presnall DC (1966) The join forsterite-diopside-iron oxide and its bearing on the crystallization of basaltic and ultramafic magmas. *Am J Sci* 264:753–809
- Presnall DC (1975) Alumina content of enstatite as a geobarometer for plagioclase and spinel lherzolites. *Am Mineral* 61:398–406
- Presnall DC, Brenner NL, O'Donnell TH (1973) Drift of Pt/Pt10Rh and W3Re/W25Re thermocouples in single stage piston-cylinder apparatus. *Am Mineral* 58:771–777
- Presnall DC, Dixon JR, O'Donnell TH, Dixon SA (1979) Generation of mid-ocean ridge tholeiites. *J Petrol* 20:3–35
- Presnall DC, Dixon SA, Dixon JR, O'Donnell TH, Brenner NL, Schrock RL, Dycus DW (1978) Liquidus phase relations on the join diopside-forsterite-anorthite from 1 atm to 20 kbar: their bearing on the generation and crystallization of basaltic magma. *Contrib Mineral Petrol* 66:203–220
- Presnall DC, Simmons CL, Porath H (1972) Changes in electrical conductivity of a synthetic basalt during melting. *J Geophys Res* 77:5665–5672
- Snyder GL (1959) Geology of Little Sitkin Island, Alaska. *US Geol Survey Bull* 1028-H:169–210
- Stolper E (1980) A phase diagram for mid-ocean ridge basalts: preliminary results and implications for petrogenesis. *Contrib Mineral Petrol* 74:13–27
- Yoder HS, Jr, Tilley CE (1962) Origin of basalt magmas: an experimental study of natural and synthetic rock systems. *J Petrol* 3:342–532

Received April 14, 1982; Accepted August 18, 1983